# *N, N*-Dimethyl Formamide Regulating Fluorescence of MXene Quantum Dots for the Sensitive Determination of $Fe^{3+}$

**Xiaohui Gao** ( xiaohuigao@csu.edu.cn )
Central South University https://orcid.org/0000-0001-7051-702X
**Xiaochun Shao**
Central South University
**Longlong Qin**
Central South University
**Yejun Li**
Central South University
**Shengxiang Huang**
Central South University
**Lianwen Deng**
Central South University

**Research Article**

**Keywords:** MQDs, X-ray photoelectron energy spectra, UV-Vis absorption, fluorescence spectra

**Posted Date:** August 3rd, 2021

**DOI:** https://doi.org/10.21203/rs.3.rs-770200/v1

# Abstract

Due to widely use of iron in all kinds of areas, the design and construction of direct, fast, and highly sensitive sensor for $Fe^{3+}$ is highly desirable and important. In the present work, a kind of fluorescent MQDs were synthesized via an intermittent ultrasound process with *N,N*-dimethyl formamide as solvent. The prepared MQDs were characterized via a combination of UV-Vis absorption, fluorescence spectra, X-ray photoelectron energy spectra, and Fourier transform infrared spectroscopy. Based on the electrostatic induced aggregation quenching mechanism, the fluorescent MQDs probes exhibited excellent sensing performance for the detection of $Fe^{3+}$, with a sensitivity of 0.6377 $mM^{-1}$ and the detection limit of 1.4 μM, superior to those reported in literatures. The present MQDs-based probes demonstrate potential promising applications as the sensing device of $Fe^{3+}$.


# Introduction

MXene quantum dots (MQDs), originating from 2D transition metal carbides or nitride MXenes, show appealing physical and chemical properties including abundant metal-deficient sites, excellent charge or electrons transport ability, and good biocompatibility, which greatly contribute to the wide range of applications in energy storage, catalysis, sensors, thermoelectricity, and bio-imaging, etc.[1–4] In recent years, in combination of the appropriate band gap, easy surface modification, and the quantum size effect, the fluorescent properties of MQDs are gradually emerging as a great application prospect in the optical-sensing field such as the detection of metal ions, hypochlorite, glutathione, hypochlorite and so on.[5–7] As reported, the performance of MQDs-based sensors substantially depends on the optical and interfacial properties of materials.[8, 9] Meanwhile, considerable research efforts have been devoted into the synthesis of MQDs and understanding the critical roles of the surface capping organic ligands and the solvents used in the synthesis process. For example, Zhou et al. synthesized nitrogen-doped $Ti_3C_2$ QDs, which combined with *2,3*-diaminephenazine and presented a sensitively ratiometric sensor for $H_2O_2$ and xanthine. The limit of detection was determined to be 0.57 and 0.34 μM, respectively.[10] By integrating the electron transfer and inner filter effect, Liu et al. reported fluorescent MQDs synthesized in dimethyl sulfoxide (DMSO) for the detection of $Fe^{3+}$ with high sensitivity and selectivity.[11] Despite of these, the current literatures about fluorescent MQDs-based sensors are still limited, while in particular the exploration of the relationship between optical and interfacial properties of MQDs is still in infancy.

Iron, as an indispensable metal, has been widely used in all kinds of areas. On one hand, large quantities of waste water containing ferric ions are constantly released to the natural environment, which is detrimental to the microorganism and the food chain.[12–14] On the other hand, the level of iron ions in blood is critical to the health of human body, and the corresponding disorder can cause the serious physiological responses, including cardiopalmus, anemia, and the dysfunction of organs.[15,16] Therefore, the accurate determination of iron content is of great importance to the sustainable development of mankind and society. To date, all kinds of analytical techniques have been utilized to the detection of

colorimetry, and electrochemistry, etc.[17–19] Among these methods, fluorometric analysis offers some unique advantages such as high sensitivity, rapid response, and good selectivity. Various fluorescent nanomaterials have also been developed for the analysis of $Fe^{3+}$, e.g., quantum dots, small molecule probes, metal-organic frameworks, and metal nanoclusters etc.[20–24] However, it is worthy to be mentioned that the existing sensitivity and selectivity remain significant challenges for in-situ and portable detection. The research and development of direct, fast, and highly sensitive probes for $Fe^{3+}$ is still desirable and important.

Therefore, in this work, a kind of fluorescent MQDs were synthesized via an intermittent ultrasound process with *N,N*-dimethyl formamide as solvent. The prepared MQDs were characterized by UV-Vis absorption, fluorescence spectra, X-ray photoelectron energy spectra, and Fourier transform infrared spectroscopy. Based on the electrostatic induced aggregation quenching mechanism, the fluorescent MQDs probes exhibited excellent sensing performance for the detection of $Fe^{3+}$. The sensitivity was determined to be 0.6377 $mM^{-1}$ with the detection limit of 1.4 μM, superior to those reported in literatures. We believe that the present MQDs-based probes will be a promising candidate for the sensing device of $Fe^{3+}$.

# Methods And Experiments

**Chemicals and materials.** Bulk titanium aluminum carbide powders ($Ti_3AlC_2$, 98%) were purchased from Beijing Forsman Scientific Co., Ltd. Hydrofluoric acid (HF, A.R., ≥ 40 %), zinc nitrate hexahydrate ($Zn(NO_3)_2.6H_2O$, A.R.), sodium chloride (NaCl, A.R.), and potassium chloride (KCl, A.R.) were brought from Sinopharm Chemical Reagent Co., Ltd (Shanghai). Iron nitrate nonahydrate ($Fe(NO_3)_3.9H_2O$, A.R.), nickel nitrate hexahydrate ($Ni(NO_3)_2.6H_2O$, A.R.), and cobalt nitrate hexahydrate ($Co(NO_3)_2.6H_2O$, A.R.) were gotten from Guangdong Guanghua Sci-Tech. Co., Ltd. *N,N*-dimethyformanide ($C_3H_7NO$, DMF, A.R.) and cupric nitrate trihydrate ($Cu(NO_3)_2.3H_2O$, A.R.) were obtained from Shanghai Macklin Biochemical Co., Ltd. Aluminum nitrate nonahydrate ($Al(NO_3)_3.9H_2O$, A.R.) was from Aladdin. Nitric acid ($HNO_3$, 65–68 %) was gotten from Chengdu Chron Chemicals Co., Ltd. Ammonium chloride ($NH_4Cl$, A.R.) and magnesium chloride hexahydrate ($MgCl_2.6H_2O$, A.R.) were brought from Shanghai Zhanyun Chemical Co., Ltd and Xilong Chemical Co., Ltd, respectively.

**Characterizations.** Transmission electron microscopy (TEM) images were collected on Titan G2 60–300 with an acceleration voltage of 300 KV. X-ray photoelectron spectroscopy (XPS) experiments were conducted on a AVG Thermo VG ESCALAB 250 spectrometer equipped with a Mg Kα anode. Fourier transform infrared (FT-IR) spectra were recorded on a BRUKE Vertex-70 FTIR spectrometer. UV-Vis spectra were obtained on a UV-3000PC spectrometer (Shanghai Mapada Instrumental Co., Ltd). Zeta potentials were measured on a Zeta Sizer Nano ZS (Malvern Instruments, UK). Fluorescence spectra were recorded by using F-4600 fluorescence spectrophotometer (Hitachi, Tokyo, Japan).

**Synthesis of MXene quantum Dots.** In a typical process, 20 ml of hydrofluoric acid was added into a Teflon container with 2 g of bulk $Ti_3AlC_2$ powders. The mixture was allowed to constantly stirring at room temperature for 48 h. During this process, the aluminum layers were etched and the primary products were collected through centrifugation and washed with plenty of ultrapure water until neutral. Subsequently, the obtained solid substances were dispersed into 50 ml of DMF, and the dispersion was intermittently sonicated for another 48 h. The yellow supernatants were collected as the final products after centrifugation and stored for further use.

**Fluorescence detection of $Fe^{3+}$ ions.** In a typical detection, $Fe(NO_3)_3$ solutions were prepared by diluting the stock solution (10 mM) with aqueous nitric solution (10 mM). Different volumes of $Fe^{3+}$ solution were mixed with 300 µL of the as-prepared MXene quantum dots solution and the fluorescence curves were measured at room temperature after 60 s. To examine the selectivity of MXene quantum dots toward $Fe^{3+}$, other metal ions with concentration of 10 mM ($Na^+$, $K^+$, $Ni^{2+}$, $Cu^{2+}$, $Co^{2+}$, $Zn^{2+}$, $Mg^{2+}$, $Al^{3+}$, and $NH_4^+$) were also tested and the corresponding changes of fluorescence intensity were recorded.

## Results And Discussion

# Synthesis and characterizations

In this work, the synthesis of MQDs was completed through the intermittent sonication for 48 h. As shown in Fig. 1, by using hydrofluoric acid as etching reagent, the bulk $Ti_3AlC_4$ powders were first transformed into $Ti_3C_2$ nanosheets, which were subsequently cut into MQDs under the assistance of ultrasound and DMF solvent. To demonstrate the successful formation of MQDs, transmission electron microscopy (TEM) experiments were performed. As shown in Fig. 2a, abundant MXene quantum dots instead of nanosheets were observed in the image, which is consistent with the previous reports.[25–27] Based on a hundred particle count, the statistical average size of the obtained MQDs was estimated to be 2.75 nm, as shown in the inset of Fig. 1a.

As reported, the optical properties are one of the most fascinating part of quantum dots. Figure 2b revealed the fluorescence properties of the synthesized MQDs. The excitation and emission wavelength was determined at 365 and 445 nm, respectively, indicating the blue fluorescence at the excitation wavelength. In Fig. 2c, the UV-Vis spectrum showed that the absorption decreases as the wavelength increases. The predominate optical absorption is below 400 nm, in agreement with the fluorescence excitation spectrum. To analyze the chemical bonds in the MQDs, Fourier transform infrared spectroscopy (FTIR) experiments were conducted. As shown in Fig. 2d, the peaks at 1462 and 1654 $cm^{-1}$ were originated from the stretching modes of C-N and C = O bond, respectively.[28,29] The signals at 2894 and 2914 $cm^{-1}$ were attributed to the C-H (-$CH_3$ and –CH = O) stretching mode, indicating surface modification of the MQDs with the DMF molecules during the ultrasound process.[30] Note that the peak at 2365 $cm^{-1}$ was resulted from the carbon dioxide in air. As well-known, X-ray photoelectron spectroscopy



ent of the elements, which can be used to analyze the

chemical valence states of elements. Figure 3a showed the survey spectrum from MQDs. As expected, the elements of Ti, C, O, and N were found in the prepared MQDs, while the absence of aluminum signals indicates the complete etching of the intermediate layers. The resolved C 1s spectrum was presented in Fig. 3b. The C-C chemical bond was considered as the primary bonding mode on the basis of the relative high intensity. Due to the introduction of DMF, the C-N chemical bonds also existed in the prepared materials, which can be illustrated by the following N 1s spectrum. As shown in Fig. 3c, the signals of both C-N-C and C-N chemical bonds were presented in N 1s spectrum at the binding energy of 400.1 and 402.3 eV, respectively. For Ti 2p spectrum (Fig. 3d), the peaks at 458.7 and 464.3 eV were attributed to the Ti $2p_{1/2}$ and Ti $2p_{3/2}$ of Ti-O bonds, respectively, in consistent with the literature results.[31, 32] Therefore, combining with the TEM image, these results further illustrated the successful formation of MQDs with the modification of DMF molecules.

# The Sensitive And Selective Detection Of Fe Ions

Based on the high fluorescence intensity, the prepared MXene quantum dots were allowed to analyze the ferric ions in aqueous solution. As shown in Fig. 4a, the fluorescence intensity of MQDs was gradually decreasing with the addition of ferric ions, indicating an effective quenching effect. In particular, approximate 30% of fluorescence intensity was suppressed by the ferric ions with the concentration of 1.4 mM. For further quantitative investigation, the fluorescence response of the MQDs towards ferric ions with different concentrations was also examined. In Fig. 3b, a linear relationship between $(F_0\text{-}F)/F$ and concentration of ferric ion was found, where the calibration equation can be fitted into: $Y = 0.6377x + 0.0113$ ($R^2 = 0.996$) (where F and $F_0$ represent the fluorescence intensity with and without the addition of ferric ions, respectively). According to the triple signal-to-noise ratio rule, the limit of detection was calculated to be 1.4 μM with a linear range from 0 to 0.8 mM, superior to the results from previous reports.[33–35] To investigate the potential quenching mechanism, zeta potential and UV-Vis spectra experiments were conducted. As shown in Fig. 4c, the zeta potential of -10.9 mV was determined for the prepared MQDs, which indicates a strong electrostatic interaction between metal ions and quantum dots. The higher positive charge of $Fe^{3+}$ induced a stronger interaction, which may play a key role in the fluorescence quenching of MQDs. UV-Vis spectra showed a pronounced decrease of the absorption intensity of the supernatant after the addition of iron, when compared to the pristine solution, as displayed in Fig. 4d. Meanwhile, in inset of Fig. 4d, the digital electronic images visualized the conspicuous precipitation. From this, it can be concluded that the iron ions induced the aggregation of MXene quantum dots, leading to the fluorescence quenching, as shown in Fig. 5a.

Fig. 4(a)Fluorescence emission spectra of MQDs with the addition of ferric ion; (b) calibration line between the concentration of $Fe^{3+}$and the fluorescence ratio; (c) the Zeta potential of the prepared MQDs; (d) UV-vis absorption spectra of MQDs with and without the addition of$Fe^{3+}$ions.

Selectivity is another important factor for evaluating the performance of sensors. Herein, to show the

cence intensity changes were investigated in the presence of

different interferences, including the metal ions of $K^+$, $Na^+$, $Mg^{2+}$, $Ni^{2+}$, $Co^{2+}$, $Cu^{2+}$, $Al^{3+}$, and $NH_4^+$. As shown in Fig. 5b, the MQDs solution containing other metal ions displayed the same light yellow under the daylight, while only fluorescence quenching was observed from the mixtures with the ferric ions under ultraviolet light. In Fig. 5c, the negligible fluorescence intensity fluctuations were found after the addition of interference metal ions (0.8 mM), when compared to that caused by the ferric ions with same concentration. Furthermore, Fig. 5c exhibited the peak value changes of fluorescence intensity from the mixtures with the same concentration of different metal ions. Compared to that of other ions, the peak values of ferric ions obviously changed, suggesting that the prepared luminous MXene quantum dots will be a promising probe for the detection of ferric ions.

# Conclusions

In summary, the MQDs with the blue fluorescence were synthesized through the facile intermittent ultrasound process in the presence of DMF solvent. Based on the electrostatic interaction between surface functional groups of quantum dots and iron ions, the sensitive and selective detection of $Fe^{3+}$ was realized in this work. Meanwhile, the electrostatic induced aggregation was also demonstrated. We believe that the obtained results will not only provide a new thought for synthesis of the MQDs, but also broaden the application areas.

# Abbreviations

MQDs: MXene quantum dots; DMF: *N,N*-dimethyformanide; 2D: two dimensional FTIR: Fourier Transformed Infrared Spectroscopy; XPS: X-ray photoelectron spectroscopy; TEM: Transmission Electron Microscopy

# Declarations

### Authors' contributions

X. Gao designed and completed the experiments; X. Shao and L. Qin drew the graphs; Y. Li discussed the experimental data and wrote the manuscript; S. Huang and L. Deng helped the discussion of the manuscript and checked the English writing.


### Funding

This work was supported by the National Key Research and Development Program of China (Grant No. 2017YFA0204600) and the National Natural Science Foundation of China (Grant No. 21902186, 11904411 and 21905305).


### Availability of data and material

The data and conclusions in this work are all showed in this paper.

### Competing interests

The authors declare no competing interests.

# References


1. Yang FM, Ge YQ, Yin T, Guo J, Zhang F, Tang X, Qiu M, Liang WY, Xu N, Wang C, Song YF, Xu SX, Xiao SS (2020) Acs Appl Nano Mater 3:11850–11860
2. Wang X, Zhang XD, Cao HY, Huang YM (2020) Journal of Materials Chemistry B 8:10837–10844
3. Tang R, Zhou SJ, Li CX, Chen R, Zhang LY, Zhang ZW, Yin LW, *Advanced Functional Materials*, 2020, 30
4. Qin JZ, Liu BJ, Lam KH, Song SJ, Li XY, Hu X (2020) Acs Sustain Chem Eng 8:17791–17799
5. Liu MW, Bai YX, He Y, Zhou J, Ge YL, Zhou JG, Song GW, *Microchim. Acta*, 2021, 188
6. Guan QW, Ma JF, Yang WJ, Zhang R, Zhang XJ, Dong XX, Fan YT, Cai LL, Cao Y, Zhang YL, Li NN, Xu Q (2019) Nanoscale 11:14123–14133
7. Liu MW, He Y, Zhou J, Ge YL, Zhou JG, Song GW (2020) Anal Chim Acta 1103:134–142
8. Guo Z, Zhu XH, Wang SG, Lei CY, Huang Y, Nie Z, Yao SZ (2018) Nanoscale 10:19579–19585
9. Yang GH, Zhao JL, Yi SZ, Wan XJ, Tang JN, *Sensor. Actuat. B-Chem.*, 2020, 309
10. Lu QY, Wang J, Li BZ, Weng CY, Li XY, Yang W, Yan XQ, Hong JL, Zhu WY, Zhou XM (2020) Anal Chem 92:7770–7777
11. Zhang QX, Sun Y, Liu ML, Liu Y (2020) Nanoscale 12:1826–1832
12. Yu HH, Fan MY, Liu Q, Su ZM, Li X, Pan QQ, Hu XL (2020) Inorg Chem 59:2005–2010
13. Qi HJ, Teng M, Liu M, Liu SX, Li J, Yu HP, Teng CB, Huang ZH, Liu H, Shao Q, Umar A, Ding T, Gao Q, Guo ZH (2019) J Colloid Interf Sci 539:332–341
14. Zhan ZY, Liang XY, Zhang XL, Jia YJ, Hu M (2019) Dalton transactions 48:1786–1794
15. Gao G, Jiang YW, Jia HR, Yang JJ, Wu FG (2018) Carbon 134:232–243
16. Atchudan R, Edison TNJI, Aseer KR, Perumal S, Karthik N, Lee YR (2018) Biosens Bioelectron 99:303–311
17. Wang XF, Shen CQ, Zhou CF, Bu YY, Yan XH, *Chem Eng J*, 2021, 417
18. Toghan A, Abd-Elsabour M, Abo-Bakr AM, *Sensor Actuat a-Phys*, 2021, 322
19. Zhao D, Liu XH, Zhao Y, Wang P, Liu Y, Azam M, Al-Resayes SI, Lu Y, Sun WY (2017) Journal of Materials Chemistry A 5:15797–15807
20. Zhang S, Zhang C, Shao XD, Guan RT, Hu YY, Zhang KY, Liu WJ, Hong M, Yue QL (2021) RSC Adv 11:17283–17290
21. Su YQ, Han C, Fu LS, Wei RX, Cui GH, *Journal of Solid State Chemistry*, 2021, 299
22. Zhang XS, Li CH, Zhao SL, Pang HY, Han Y, Luo XL, Tang WZ, Li ZH, *Opt Mater*, 2020, 110
23. Yang SL, Liang D, Zhao JL, *Appl Surf Sci*, 2020, 528

24. Wu P, Liu Y, Liu Y, Wang J, Li Y, Liu W, Wang J (2015) Inorg Chem 54:11046–11048
25. Xu Q, Ma JF, Khan W, Zeng XB, Li N, Cao Y, Zhao XL, Xu M (2020) Chem Commun 56:6648–6651
26. Shao JD, Zhang J, Jiang C, Lin J, Huang P, *Chem Eng J*, 2020, 400
27. Neupane GP, Wang BW, Tebyetekerwa M, Nguyen HT, Taheri M, Liu BQ, Nauman M, Basnet R, *Small*, 2021, 17
28. Gao X, Lu Y, Zhang R, He S, Ju J, Liu M, Li L, Chen W, J Mater Chem C, 2015, DOI:10.1039/C4TC02582B
29. Lu Y, Jiang Y, Wei W, Wu H, Liu M, Niu L, Chen W (2012) J Mater Chem 22:2929–2934
30. Lu YC, Chen J, Wang AJ, Bao N, Feng JJ, Wang WP, Shao LX (2015) J Mater Chem C 3:73–78
31. Pan ZH, Cao F, Hu X, Ji XH (2019) Journal of Materials Chemistry A 7:8984–8992
32. Ge J, Li W, He X, Chen H, Fang W, Du X, Li Y, Zhao L, *Mater Today Energy*, 2020, 18
33. Aslandas AM, Balci N, Arik M, Sakiroglu H, Onganer Y, Meral K (2015) Appl Surf Sci 356:747–752
34. Li GM, Lv N, Bi WZ, Zhang JL, Ni JZ (2016) New J Chem 40:10213–10218
35. Roy N, Dutta A, Mondal P, Paul PC, Singh TS (2016) Sensor Actuat B-Chem 236:719–731

# Figures

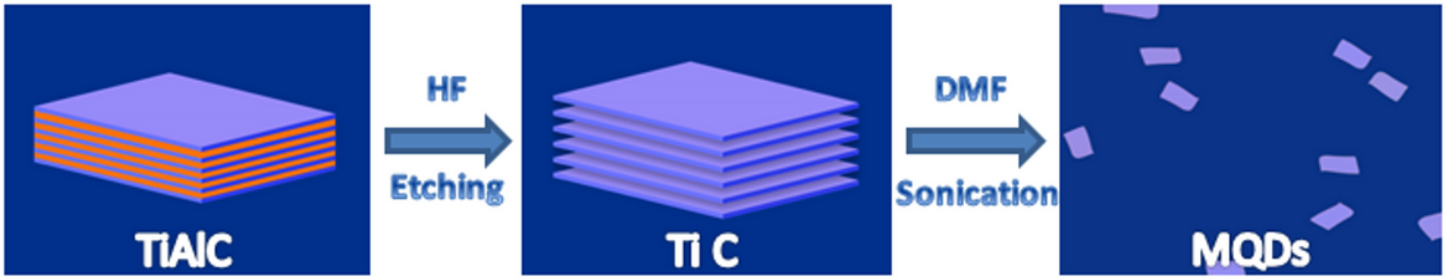


**Figure 1**

Schematic diagram for the preparation of MQDs

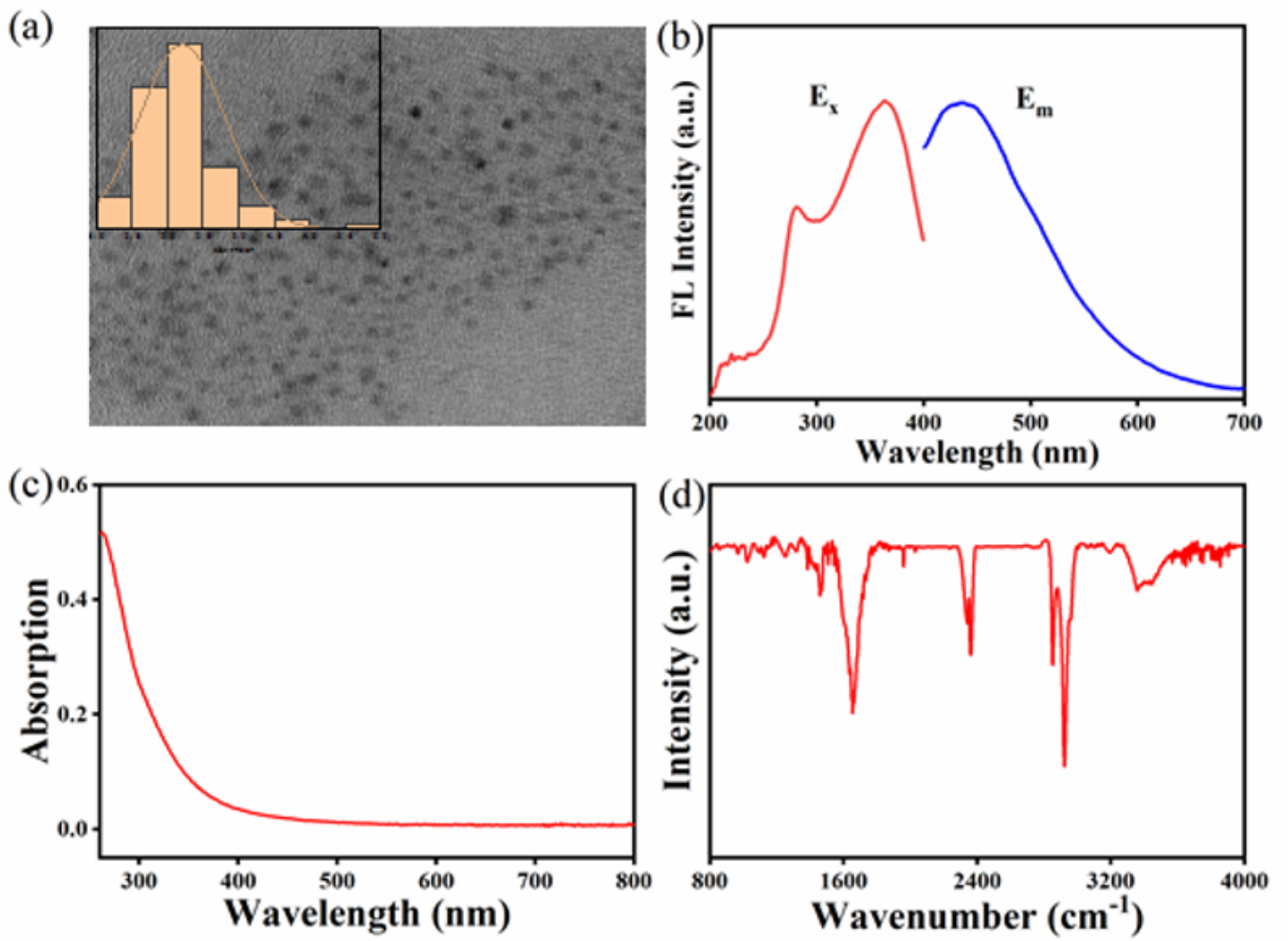


## Figure 2

(a) TEM image of the synthesized MQDs with quasi-normal distribustion of particle's size image (inset); (b) Fluorescence emission spectra of the prepared MQDs; (c) UV-vis absorption spectrum and (d) FTIR spectrum of MQDs.

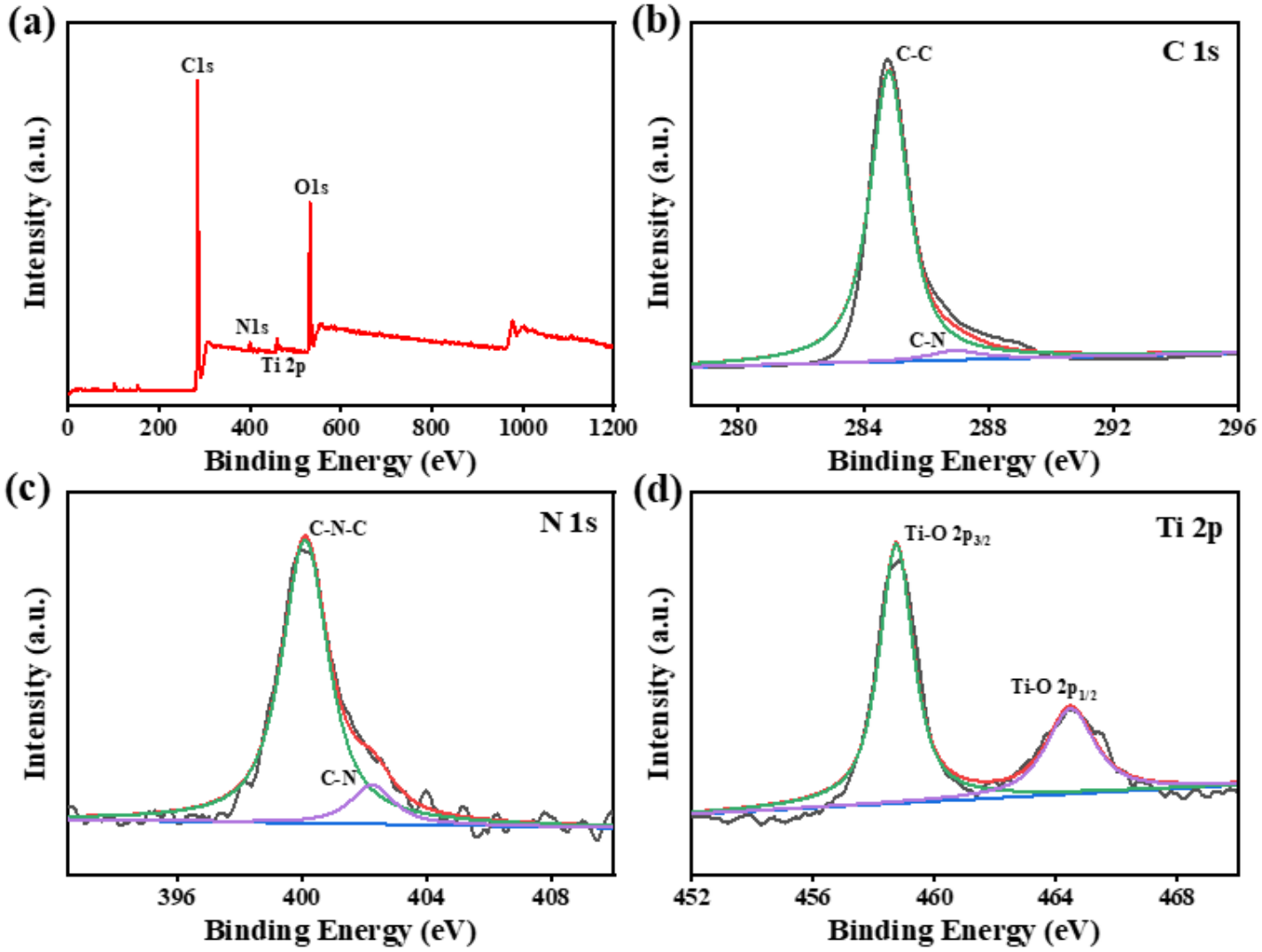


## Figure 3

(a) XPS survey spectrum of MQDs; high resolution (b) C 1s, (c) N 1s, and (d) Ti 2p XPS spectra of MQDs.

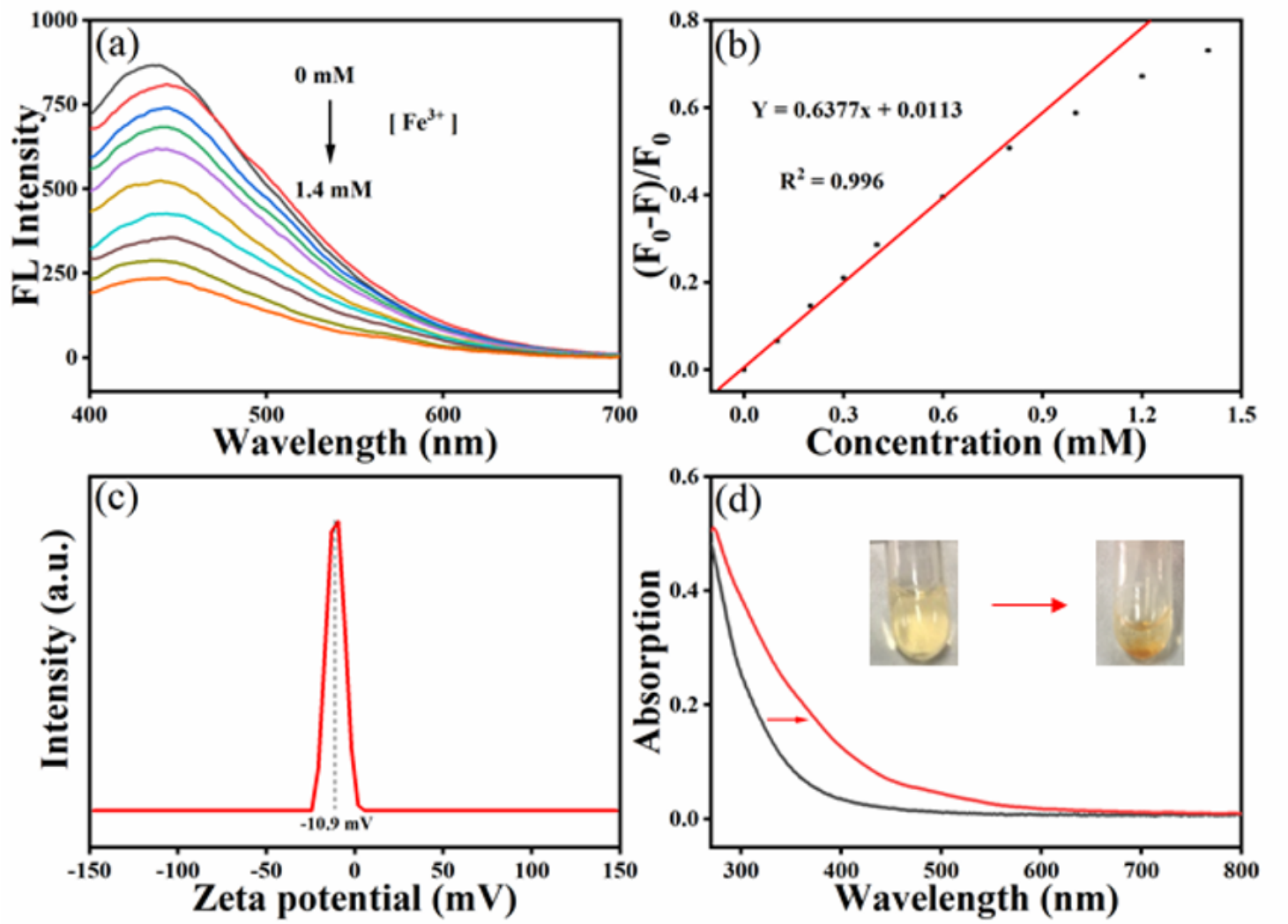


## Figure 4

(a) Fluorescence emission spectra of MQDs with the addition of ferric ion; (b) calibration line between the concentration of Fe3+ and the fluorescence ratio; (c) the Zeta potential of the prepared MQDs; (d) UV-vis absorption spectra of MQDs with and without the addition of Fe3+ions.

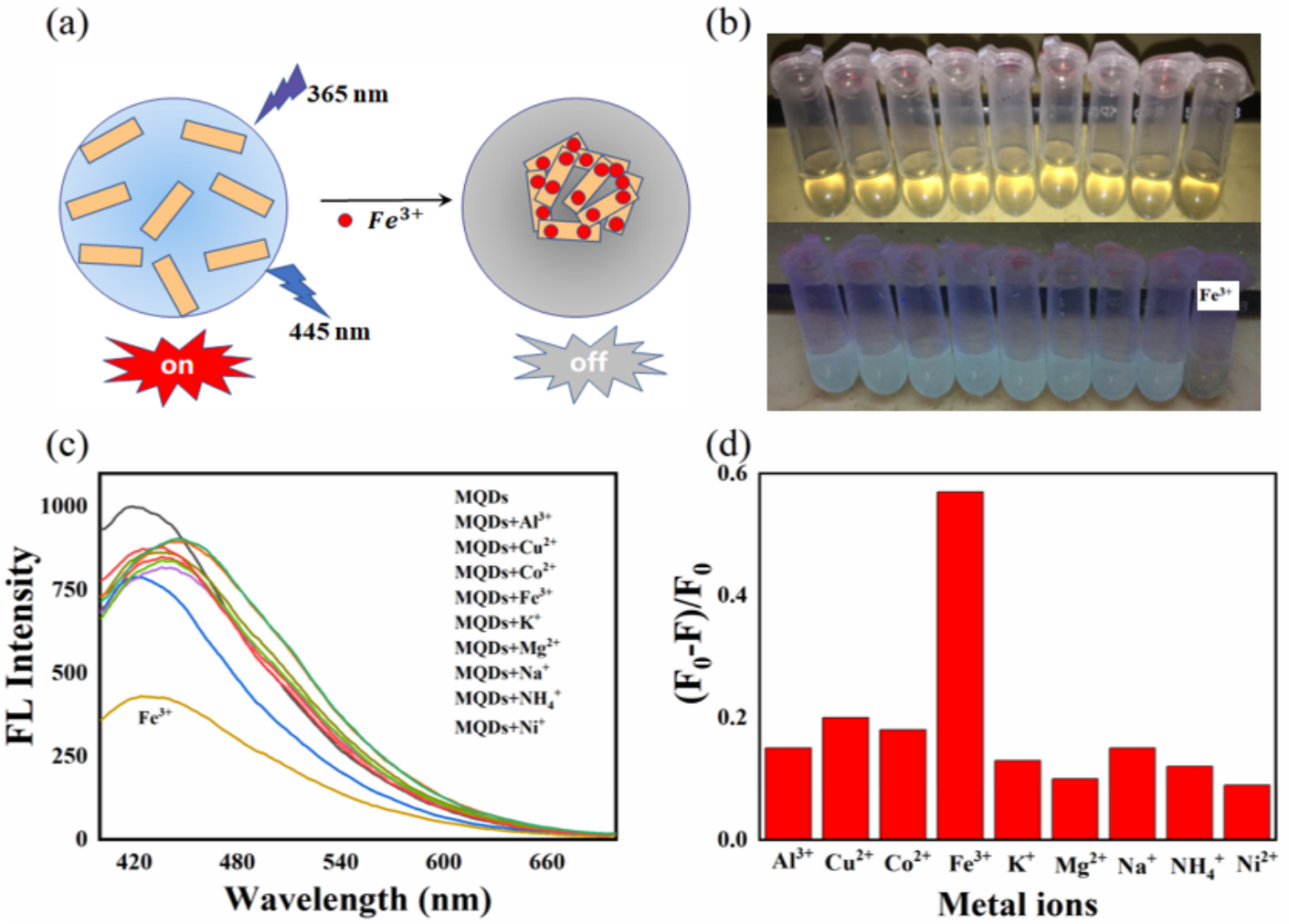


## Figure 5

(a) Schematic diagram for the fluorescence quenching mechanism of MQDs by ferric ions; (b) the picture for the MQDs solutions with the addition of different metal ions (0.8 mM) under the visible and ultraviolet light; (c) the fluorescent curves of MQDs solution with the different metal ions (0.8 mM); (d) the fluorescent intensity change of MQDs towards different metal ions collected from the curves in (c).